Solidification of PCM around Curved Tubes Including Natural Convection Effects

K. A. R. Ismail[1*], L. M. Sousa[2], F. A. M. Lino[3]

[1, 2, 3]State University of Campinas, Faculty of Mechanical Engineering, Rua Mendeleiev, 200, Cidade Universitária Zeferino Vaz, Barão Geraldo, Campinas, 13083-860, S. P., Brazil

[*1]kamal@fem.unicamp.br

***Abstract*-This paper presents the results of a numerical study on the solidification of PCM around a bent tube with a cooling fluid flow inside it. The proposed model is based on the two-dimensional energy and momentum equations. The Landau interface immobilization technique is used to immobilize the solid-liquid interface, while the finite volume method is used to numerically treat the equations, boundary, and initial conditions. The numerical predictions were validated against available experimental results, showing good agreement. Because of the circulatory flow in the bend region, the heat transfer coefficient on the external side is higher than that on the internal side of the bent tube. It was found that an increase of the wall temperature, an increase of the initial liquid PCM temperature, or an increase of the curvature radius would reduce the interface position and consequently reduce the solidified mass and decrease the interface velocity. This increases the time for complete solidification. These results can be useful in predicting ice formation over helical coils and curved tubes used in latent heat storage systems.**

Keywords- PCM; Solidification; Curved Tubes; Interface Immobilization; Latent Heat Storage; Coiled Tubes

I. INTRODUCTION

In the last few decades, energy generation and its efficient utilization has occupied the top place in the lists of priorities of many countries. In most cases, energy generation and efficient utilization is highly tied to the need for equipment for energy storage, as this equipment is a vital tool for accomplishing these objectives, especially when handling intermittent and non-conventional systems. In applications where thermal energy is involved, thermal energy storage techniques are highly preferred. Thermal storage can be accomplished basically by three means: sensible heat storage, latent heat storage, and hybrid storage involving latent and sensible heats. Latent heat storage is most preferred because of its high energy storage capacity and its constant temperature during the charging and discharging processes. Many studies have been reported on the numerical models and experimental results of models and applications of latent heat storage. In contrast, a scarce number of studies have been reported on spiral and bent tubes, including either internal or external phase changes.

Although heat transfer and fluid flow inside curved tubes have been studied for many decades, the inclusion of phase change in this type of problem is relatively recent. The growing interest in the subject is mainly due to its importance in latent heat storage applications. The internal vortices, recirculation flow, and agitation associated with flow in a tube bend provoke intense and different heat transfer coefficients on the two sides of the bend. This causes an increase of the external local heat transfer coefficient in comparison with that of the internal side, and this increases the solidified mass on the external side. For this and other reasons, it is important to investigate the process of heat transfer with phase changes in bent and curved tubes.

Dean [1] published the results of a theoretical study of flow inside curved tubes and showed that the flow rate is controlled by a parameter he named after himself, the Dean number. He developed later what is called “loose coil approximation” to be used when the curvature radius is very large. A pioneer study on heat transfer in curved tubes was performed by [2], who found a completely developed temperature profile inside a curved tube. The results for water showed a temperature profile totally different from that found in straight tubes. He found that the local heat transfer coefficient on the external side of the curved tube is more than that on the internal side.

Kubair and Kuloor [3] investigated the pressure drop and heat transfer in the laminar flow of glycerol in different helicoidal and spiral geometries. Ozisik and Topakoglu [4] investigated laminar heat transfer in curved tubes and found that the heat transfer process depends upon three parameters, that is, the Reynolds number, the Prandtl number, and the radius of the curvature of the bend. They also found that the local heat transfer coefficient is higher in the outer surface of the tube than for the inner surface and that the temperature gradient across the wall is higher at the outer surface than in the inner surface, confirming the findings of [2].

Theoretical treatments of heat transfer in curved tubes with completely developed velocity and temperature fields were presented by [5] and [6], who used toroidal coordinates in the formulation of the problem, and the resulting system of equations was approximated by finite differences. They were able to determine the peripheral Nusselt number and the ratio of the external to the internal local heat transfer coefficients on the two sides of the curved tube.

Patankar, Pratap, and Spalding [7] studied the three-dimensional laminar flow in spiral tubes for the case of the long radius of the curvature and in the region of developing hydrodynamic and thermal flow fields.

DOI: 10.5963/IJEE0503002

Janssen and Hoogendoom [8] confirmed the presence of secondary flow in curved tubes and its effect on increasing heat and mass transfer when compared with straight tubes under the same conditions. They investigated two boundary conditions of average uniform heat flux and constant wall temperature.

Yang and Chang [9] numerically studied heat transfer in curved tubes with different curvature ratios and analyzed the effects of the curvature radius, friction ratio, Reynolds number, and Prandtl number. Their findings agreed well with the work of [4].

Yang and Ebadian [10] analytically solved the laminar problem of convection heat transfer in a spiral tube. The equations of continuity and momentum in the radial, axial, and tangential directions were solved uncoupled from the energy equation. The authors were able to determine the tangential Nusselt number.

Braun and Beer [11] performed a numerical study on the solidification of flowing water inside a curved channel of a square cross section under turbulent conditions. They found that the ice layer along the channel periphery was not symmetrical, due to the different characteristics at the internal and external sides of the channel.

Nobari and Amani [12] numerically solved the flow problem with heat transfer in a curved tube by using toroidal coordinates. They analyzed the effects of curvature, the Reynolds number, the Prandtl number, and curvature ratios, and found good agreement with available results.

Ismail et al. [13] experimentally and numerically studied the solidification of PCM around a curved tube. Their proposed model is based on pure conduction. They investigated the effects of the temperature of the working fluid, curvature ratio, and working fluid flow rate on the interface position, interface velocity, and the solidified mass fraction. The numerical predictions agreed well with the experimental results.

Kurnia et al. [14] numerically investigated various configurations of PCM thermal storage devices based on U tube configuration with and without fins. They solved the conjugate heat transfer problem between the heat transfer fluid and PCM by using the CFD approach and utilizing enthalpy-porosity formulation.

From the literature review, it is clear that reported studies on flow and heat transfer in curved tubes and coils are very limited. The inclusion of phase change makes the combined flow and heat problem more complex, as indicated by the limited experimental and numerical results available. Kurnia et al. [14] is the nearest to the present study; they used the CFD approach for their investigation. The present study treats the problem of solidification outside a bent tube submersed in PCM, allowing convection in the liquid phase of the PCM. In this study a two-dimensional convection model is adopted. This model is based on the energy and momentum equations for the flow and heat transfer in a curved tube submerged in a stagnant PCM at a fixed initial temperature. The moving interface is fixed by using the Landau transform, which immobilized the moving front. The basic equations, the associated boundary, and the initial conditions were discretized by using the finite volume method. The numerical predictions were validated against experimental results, and good agreement was found. Additional numerical results were obtained to determine how the interface position, the time for complete solidification, and the solidified mass are influenced by varying the geometrical and operational parameters of the problem.

II. FORMULATION OF THE PROBLEM

The physical problem under investigation is composed of a bent tube fully submersed in liquid PCM, initially at a constant temperature different from its phase change temperature, as in Fig. 1a. The PCM used in this study is water. This does not impose any restrictions to the proposed model. A cold fluid at a temperature less than the phase temperature is allowed to flow in the bent tube. As a result of the temperature gradient between the circulating cold fluid and the PCM, the sensible heat is gradually removed. When the first layer of the PCM in contact with the tube's external surface reaches the phase change temperature, the layer solidifies. With the increase of time, the solidified front advances towards the liquid PCM. A mathematical model must be formulated to describe this process and predict the interface position, velocity, and solidified mass at any instant.

To formulate the mathematical model, the following assumptions and simplifications are considered:

1) The model is transient and two dimensional;
2) Natural convection effects in the liquid PCM are considered;
3) The thermo-physical properties of the PCM are considered constants, except its density;
4) The fluid is Newtonian and incompressible;
5) The phase change material in the solid phase is at a uniform temperature equal to the phase change temperature.

A. Governing Equation in the Liquid and Solid Phases

The solid phase is surrounded by the sides AB, BC, CD, and DA. Fig. 1b and the equations are given by:

DOI: 10.5963/IJEE0503002

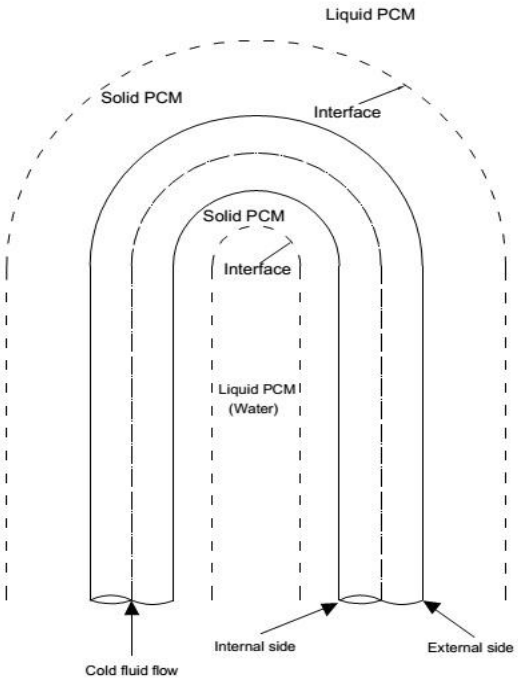

(a)

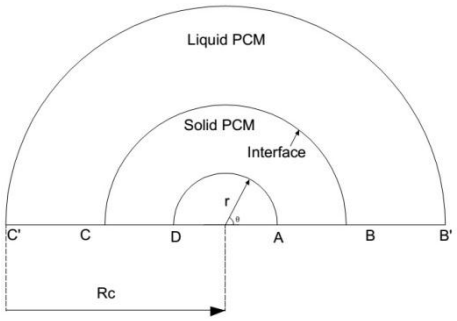

(b)

Fig. 1 Layout of the problem

$$\frac{1}{rB}\left(\frac{\partial}{\partial r}\left(rBV_r\right)+\frac{\partial}{\partial \theta}\left(BV_\theta\right)\right)=0 \tag{1}$$

$$\frac{\partial V_r}{\partial t}+\frac{1}{rB}\left[\frac{\partial}{\partial r}\left(rBV_r^2\right)+\frac{\partial}{\partial \theta}\left(BV_rV_\theta\right)-BV_\theta^2\right]=-\frac{1}{\rho}\frac{\partial P}{\partial r}+\overline{\Lambda}\sin\theta$$
$$+\nu\left\{\frac{1}{rB}\left[\frac{\partial}{\partial r}\left(rB\frac{\partial V_r}{\partial r}\right)+\frac{\partial}{\partial \theta}\left(\frac{B}{r}\frac{\partial V_r}{\partial \theta}\right)\right]-\frac{1}{r^2}\left(2\frac{\partial V_\theta}{\partial \theta}+V_r\right)+\right. \tag{2}$$
$$\left.+\frac{V_\theta\sin\theta}{rB}+\frac{\cos\theta}{B^2}\left(V_\theta\sin\theta-V_r\cos\theta\right)\right\}$$

$$\frac{\partial V_\theta}{\partial t}+\frac{1}{rB}\left[\frac{\partial}{\partial r}\left(rBV_rV_\theta\right)+\frac{\partial}{\partial \theta}\left(BV_\theta^2\right)+BV_rV_\theta\right]=-\frac{1}{\rho}\frac{1}{r}\frac{\partial P}{\partial \theta}+\overline{\Lambda}\cos\theta+$$
$$+\nu\left\{\frac{1}{rB}\left[\frac{\partial}{\partial r}\left(rB\frac{\partial V_\theta}{\partial r}\right)+\frac{\partial}{\partial \theta}\left(\frac{B}{r}\frac{\partial V_\theta}{\partial \theta}\right)\right]+\frac{1}{r^2}\left(2\frac{\partial V_r}{\partial \theta}-V_\theta\right)-\right. \tag{3}$$
$$\left.\frac{V_r\sin\theta}{rB}-\frac{\sin\theta}{B^2}\left(V_\theta\sin\theta-V_r\cos\theta\right)\right\}$$

DOI: 10.5963/IJEE0503002

$$\frac{\partial T_2}{\partial t} + \frac{1}{rB}\left[\frac{\partial}{\partial r}\left(rBV_r T_2\right) + \frac{\partial}{\partial \theta}\left(BV_\theta T_2\right)\right] = \alpha_2\left\{\frac{1}{rB}\left[\frac{\partial}{\partial r}\left(rB\,\frac{\partial T_2}{\partial r}\right) + \frac{\partial}{\partial \theta}\left(\frac{B}{r}\,\frac{\partial T_2}{\partial \theta}\right)\right]\right\} \tag{4}$$

In the liquid phase, surrounded by the sides BB', B'C', C'C, and CB, the energy equation can be written as:

$$\frac{\partial T_1}{\partial t} = \alpha_1\left\{\frac{1}{rB}\left[\frac{\partial}{\partial r}\left(rB\,\frac{\partial T_1}{\partial r}\right) + \frac{\partial}{\partial \theta}\left(\frac{B}{r}\,\frac{\partial T_1}{\partial \theta}\right)\right]\right\} \tag{5}$$

where V_r and V_θ are the radial and tangential velocities, respectively; r and θ are the radial and tangential coordinates; $T_{1,2}$ are the temperatures of the solid and liquid phase; $\alpha_{1,2}$ are the thermal diffusivities of the solid and liquid phase; ρ is the liquid phase density; ν is the kinematic viscosity; β is the coefficient of thermal expansion; P is the pressure; and $B = Rc + r\cos\theta$. In equations (2) and (3), the adopted PCM is water and hence

$$\overline{\Lambda} = \frac{rsp \cdot g\left|T_2 - T_{ref}\right|^{1,894816}}{\left(1 - rsp \cdot \left|T_{mean} - T_{ref}\right|^{1,894816}\right)}$$

B. Boundary and Initial Conditions

The boundary conditions of Fig. 1b are defined as below:

a) Tube wall – side AD

$$\left.\begin{aligned} T &= T_p \\ k_1\,\frac{\partial T_1}{\partial r} &= q \end{aligned}\right\} \text{ at } r = r_p,\ t > 0 \tag{6}$$

b) Symmetry – side (AB and CD)

$$\frac{\partial T}{\partial \theta} = 0 \text{ at } \theta = 0 \text{ and } \pi,\ t > 0; \tag{7}$$

c) Solid – liquid interface – side BC

$$\left.\begin{aligned} T_1 &= T_2 = T_m \\ V_r &= 0 \\ V_\theta &= 0 \end{aligned}\right\} \text{ at } r = r_i(t), \text{ (initial condition)} \tag{8}$$

Energy balance at the phase change interface must be satisfied:

$$\left[1 + \left(\frac{1}{r_1}\,\frac{\partial r_1}{\partial \theta}\right)^2\right]\left(k_1\,\frac{\partial T_1}{\partial r_1} - k_2\,\frac{\partial T_2}{\partial r_2}\right) = \rho L\,\frac{dr_i}{dt} \text{ in the } r = r_i(t),\ t > 0 \tag{9}$$

d) Symmetry – side (BB' and C'C)

$$\left.\begin{aligned} \frac{\partial T}{\partial \theta} &= 0 \\ \frac{\partial V_r}{\partial \theta} &= 0 \\ V_\theta &= 0 \end{aligned}\right\} \text{ at } \theta = 0 \text{ and } \pi,\ t > 0; \tag{10}$$

e) Liquid interface, symmetry circle – side B'C'

DOI: 10.5963/IJEE0503002

$$\left.\begin{array}{l} T = T_\infty \\ \dfrac{\partial V_r}{\partial r} = 0 \\ \dfrac{\partial V_\theta}{\partial r} = 0 \end{array}\right\} \text{ at } r = R_c \text{, (initial condition)} \tag{11}$$

C. Interface Immobilization Technique

The existence of a domain with an irregular moving front unknown a priori makes the solution of the problem of phase change complicated. In order to avoid this difficulty, the front immobilizing technique is used. In this case, the physical problem, Fig. 1, in the radial and angular coordinate system is transformed to the new plane in the coordinate system η and θ. With this transformation, the solid liquid front becomes stationary and parallel. The new coordinate system in dimensionless form is given by:

$$\eta_1 = \frac{r - r_p}{r_i(t) - r_p};\ \eta_2 = \frac{r - r_i(t)}{R_o - r_i(t)} \tag{12}$$

In the new system of coordinates, the domain of the problem is limited by $0 \le \eta_{1,2} \le 1$ and $0 \le \theta \le \pi$. The surfaces of the cylinder and the solid liquid interface are defined by the constant values $\eta_1 = 0$ and $\eta_1 = 1$, respectively. In the liquid phase, they are defined by $\eta_2 = 0$, which corresponds to the solid liquid interface, and $\eta_2 = 1$ and can be considered the liquid interface at infinity.

To facilitate the mathematical treatment of the problem, the following dimensionless variables are introduced:

$$R = \frac{r}{r_p};\ R_i = \frac{r_i(t)}{r_p};\ \delta = \frac{R_c}{r_p} \tag{13a}$$

$$\eta_1 = \frac{R_1 - 1}{\Delta_1};\ \eta_2 = \frac{R_2 - R_i(\tau)}{\Delta_2} \tag{13b}$$

$$\Delta_1 = R_i(\tau) - 1;\ \Delta_2 = \delta - R_i(\tau) = \delta - 1 - \Delta_1 \tag{13c}$$

$$R_1 = \eta_1 \Delta_1 + 1;\ R_2 = \eta_2 \Delta_2 + R_i(\tau) \tag{13d}$$

$$\left.\begin{array}{l} \tau = \dfrac{\alpha_2 t}{r_p^2} Ste \\ H = \dfrac{T - T_m}{T_m - T_p} \end{array}\right\};\ \left.\begin{array}{l} \tau = \dfrac{\alpha_2 t}{r_p^2} Ste_q \\ H = \dfrac{(T - T_m)k}{q r_p} \end{array}\right\} \tag{13e}$$

$$U = \frac{V_r r_p}{\alpha_2};\ V = \frac{V_\theta r_p}{\alpha_2};\ P = \frac{p r_p^2}{\rho {\alpha_2}^2};\ b = \frac{B}{r_p} = \delta + R\cos\theta \tag{13f}$$

$$Ste = \frac{C_p(T_m - T_p)}{L};\ Ste_q = \frac{C_p q r_p}{Lk} \tag{13g}$$

$$Ra_{água} = \frac{g\beta \left|T_m - T_p\right|^{1,894816} r_p^3}{\nu\alpha\left(1 - rsp\left|T_{mean} - T_{ref}\right|^{1,894816}\right)} \tag{13h}$$

$$\mathrm{Pr} = \frac{\nu}{\alpha_2} \tag{13i}$$

DOI: 10.5963/IJEE0503002

Substituting the new variables into equations (1-5) and into the boundary conditions equations (6-11), one can obtain the governing equations and the boundary conditions in the transformed plane, as below:

- ***Governing Equations in Liquid and Solid Phase***

$$\frac{1}{Rb}\frac{1}{\Delta_2}\frac{\partial}{\partial\eta}\left(RbU\right)+\frac{1}{Rb}\frac{\partial}{\partial\theta}\left(bV\right)-\Omega_{cm}=0 \tag{14}$$

$$Ste\,\frac{\partial U}{\partial\tau}+\frac{1}{Rb}\left[\frac{1}{\Delta_2}\frac{\partial}{\partial\eta}\left(RbU^2\right)+\frac{\partial}{\partial\theta}\left(bUV\right)\right]=-\frac{1}{\Delta_2}\frac{\partial p}{\partial\eta}+\Pr\left\{\frac{1}{Rb}\left[\frac{1}{\Delta_2^2}\frac{\partial}{\partial\eta}\left(Rb\frac{\partial U}{\partial\eta}\right)+\right.\right.$$
$$\left.\left.+\frac{\partial}{\partial\theta}\left(\frac{b}{R}\frac{\partial U}{\partial\theta}\right)\right]\right\}+\Omega_{rad}+\Psi_{rad} \tag{15}$$

$$Ste\frac{\partial V}{\partial\tau}+\frac{1}{Rb}\left[\frac{1}{\Delta_2}\frac{\partial}{\partial\eta}\left(RbUV\right)+\frac{\partial}{\partial\theta}\left(bV^2\right)\right]=-\frac{1}{R}\frac{\partial p}{\partial\theta}+\Pr\left\{\frac{1}{Rb}\left[\frac{1}{\Delta_2^2}\frac{\partial}{\partial\eta}\left(Rb\frac{\partial V}{\partial\eta}\right)+\right.\right.$$
$$\left.\left.+\frac{\partial}{\partial\theta}\left(\frac{b}{R}\frac{\partial V}{\partial\theta}\right)\right]\right\}+\Omega_{ang}+\Psi_{ang} \tag{16}$$

$$Ste\frac{\partial H_2}{\partial\tau}+\frac{1}{Rb}\left[\frac{1}{\Delta_2}\frac{\partial}{\partial\eta}\left(RbUH_2\right)+\frac{\partial}{\partial\theta}\left(bVH_2\right)\right]=\frac{1}{Rb}\left[\frac{1}{\Delta_2^2}\frac{\partial}{\partial\eta}\left(Rb\frac{\partial H_2}{\partial\eta}\right)+\right.$$
$$\left.+\frac{\partial}{\partial\theta}\left(\frac{b}{R}\frac{\partial H_2}{\partial\theta}\right)\right]+\Omega_{liquid} \tag{17}$$

$$Ste\frac{\partial H_1}{\partial\tau}=\frac{\alpha_1}{\alpha_2}\frac{1}{Rb}\left[\frac{1}{\Delta_1^2}\frac{\partial}{\partial\eta}\left(Rb\frac{\partial H_1}{\partial\eta}\right)+\frac{\partial}{\partial\theta}\left(\frac{b}{R}\frac{\partial H_1}{\partial\theta}\right)\right]+\Omega_{sold} \tag{18}$$

More details of the terms Ω_{cm}, Ω_{ang}, Ω_{rad}, Ψ_{ang}, Ψ_{rad}, Ω_{solid}, and Ω_{liquid} can be found in [16].

- ***Boundary and Initial Conditions***

$$\left.\begin{aligned}H_1&=-1\\\frac{1}{\Delta_1}\frac{\partial H_1}{\partial\eta}&=1\end{aligned}\right\}\quad \eta_1=0;\ \tau>0 \tag{19}$$

$$\frac{\partial H_1}{\partial\theta}=0 \text{ at } \theta=0,\pi,\ \tau>0 \tag{20}$$

$$\left.\begin{aligned}H_1&=H_2=0\\U&=0\\V&=0\end{aligned}\right\} \text{ at } \eta_1=1 \text{and } \eta_2=0\ \tau>0 \tag{21}$$

$$\left[1+\frac{1}{\left(\Delta_1+1\right)^2}\left(\frac{\partial\Delta_1}{\partial\theta}\right)^2\right]\left(\frac{1}{\Delta_1}\frac{\partial H_1}{\partial\eta}-\frac{k_1}{k_2}\frac{1}{\Delta_2}\frac{\partial H_2}{\partial\eta}\right)=\frac{\alpha_2}{\alpha_1}\frac{d\Delta_1}{\partial\tau} \tag{22}$$

$$\left.\begin{aligned}\frac{\partial U}{\partial\theta}&=0\\V&=0\\\frac{\partial H_2}{\partial\theta}&=0\end{aligned}\right\} \text{ at } \theta=0,\pi,\ \tau>0 \tag{23}$$

DOI: 10.5963/IJEE0503002

$$\left.\begin{aligned} H_o &= \frac{T_o - T_m}{T_m - T_p} = 0 \\ \frac{\partial U}{\partial \eta} &= 0 \\ \frac{\partial V}{\partial \eta} &= 0 \end{aligned}\right\} \eta_2 = 1;\ \tau > 0 \qquad (24)$$

III. NUMERICAL TREATMENT

Equations (14) to (24) of the model and its boundary and initial conditions are approximated by the method of finite volumes, using the grid in η and θ, as shown Fig. 2.

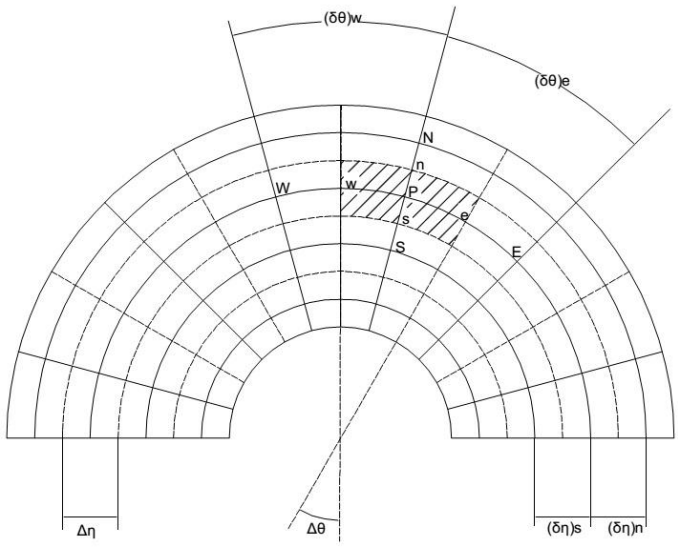

Fig. 2 Representation of the computational grid

To discretize the equations, a dislocated scheme is considered, where the continuity equation is integrated over the original control volumes, and the momentum equation is integrated over the dislocated control volumes to avoid pressure oscillations when using the co-localized scheme [17].

To handle the convective and diffusive terms in the energy and momentum equations, we used interpolating functions of the type Power-law and totally implicit formulation to treat the transient terms'.

Due to the strong coupling between pressure and velocity, the method SIMPLE [18] and the explicit scheme are used for the energy balance at the interface [16].

A flow chart for the solution procedure is shown in Fig. 3. More details about the numerical treatment can be found in [16].

Numerical trials were realized to optimize the computational grid. The number of grid points along the radial directions of 30, 50, 70, 90, and 100 were tested, and 70 grid points were chosen because of computational time, according to Fig. 4. The number of points in the angular directions of 10, 20, 30, 35, and 40 were tested, and from Fig. 5, an angular grid of 40 grid points was chosen.

The time step was chosen as 10^{-4}, since for greater values the solution showed divergence and for smaller values the computation was excessive.

In the numerical calculations, the acceptable convergence criteria parameters were based on Patankar [17, 18], as below:

- For temperature in the liquid and solid phase, we assumed convergence of 10^{-5} or less,
- For the velocity fields of U, V, we assumed convergence of 10^{-4} or less,
- For the pressure field, we assumed convergence of 10^{-3} or less.

DOI: 10.5963/IJEE0503002

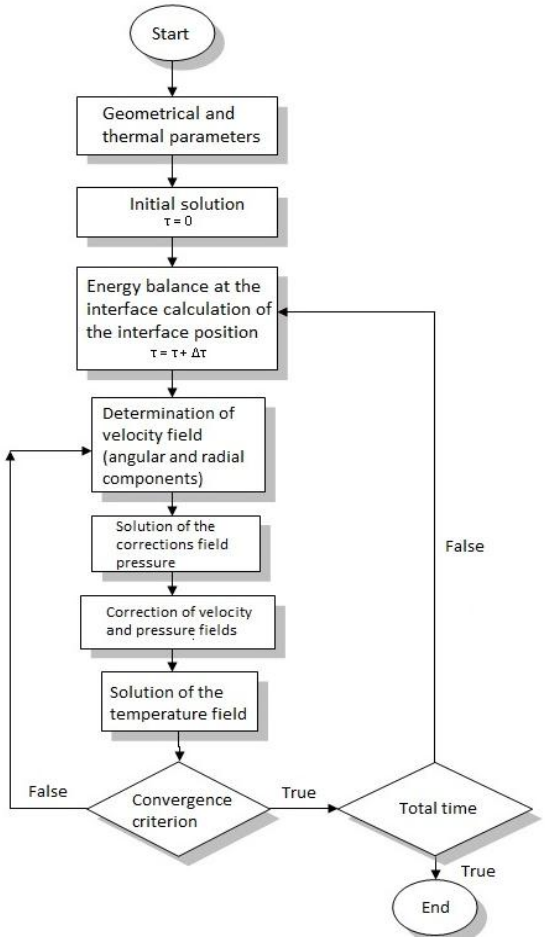

Fig. 3 Flow chart of the numerical program

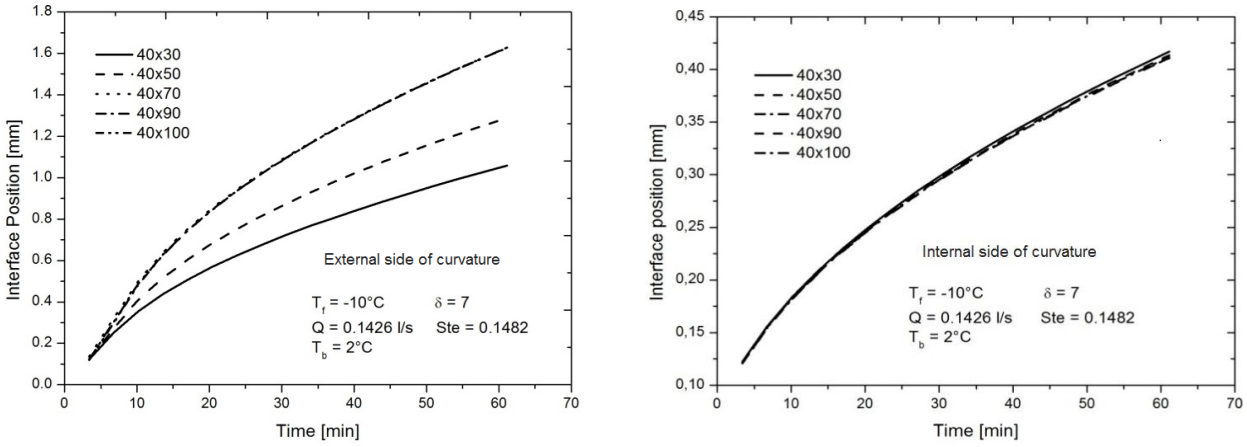

(a) External side of curvature (b) Internal side of curvature

Fig. 4 Optimization of grid size in the radial direction

DOI: 10.5963/IJEE0503002

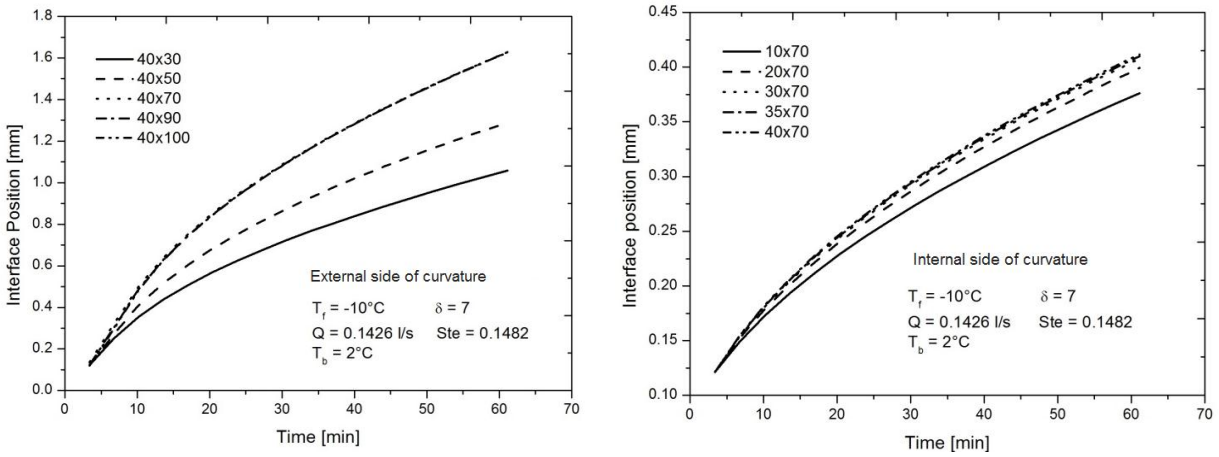

(a) External side of curvature (b) Internal side of curvature

Fig. 5 Optimization of grid size in the angular direction

IV. RESULTS AND DISCUSSION

In order to validate the model and the numerical predictions, the same test conditions were used in the numerical simulations. The numerical program works with any PCM whose physical properties are available. Water was used in the experiments as the PCM; hence, the simulations were realized with water. The properties of water and ice were obtained from correlations available in Bejan [22] p. 67 and reproduced here for reference.

The bent tube was made of copper and has a diameter of ½ inches and properties as shown in Table 2.

TABLE 1 CORRELATIONS FOR CALCULATING THE PHYSICAL PROPERTIES OF WATER, BEJAN [22]

$C_p(T) = -2.7637\cdot10^{-9}T^7 + 5.3908\cdot10^{-7}T^6 - 4.3291\cdot10^{-5}T^5 + 0.0018T^4 - 0.0504T^3 + 0.8724T^2 - 9.3434T + 4229.5069$ [J/kg-℃]

$\beta(T) = -3.4386\cdot10^{-11}T^4 + 5.3332\cdot10^{-9}T^3 - 3.6358\cdot10^{-7}T^2 + 1.9858\cdot10^{-5}T - 7.9782\cdot10^{-5}$ [1/℃]

$\rho(T) = 3.4188\cdot10^{-5}T^3 - 0.00741T^2 + 0.0476T + 999.9611$ [kg/m³]

$\mu(T) = 1.3825\cdot10^{-10}T^4 - 2.1217\cdot10^{-8}T^3 + 1.4356\cdot10^{-6}T^2 - 6.0785\cdot10^{-5}T + 0.00179$ [kg/m-s]

$\upsilon(T) = 1.4184\cdot10^{-13}T^4 - 2.1668\cdot10^{-11}T^3 + 1.4550\cdot10^{-9}T^2 - 6.0945\cdot10^{-8}T + 1.791\cdot10^{-6}$ [m²/s]

$k(T) = 9.0909\cdot10^{-10}T^4 - 1.3906\cdot10^{-7}T^3 - 2.6890\cdot10^{-6}T^2 + 0.0020T + 0.5475$ [W/m-℃]

$\alpha(T) = -2.5174\cdot10^{-15}T^4 - 2.8295\cdot10^{-13}T^3 - 1.2710\cdot10^{-11}T^2 + 7.0183\cdot10^{-10}T + 1.2952\cdot10^{-7}$ [m²/s]

$L(T) = 2.1333\cdot10^{-1}T^4 + 7.3333T^3 + 9.6666\cdot10^{1}T^2 + 5.3066\cdot10^{3}T + 3.334\cdot10^{5}$ [J/kg]

Properties of water in the solid phase

$\rho_{solid} = 917$ [kg/m³]

$C_{p_{solid}} = 2162$ [J/kg℃]

$k_{solid} = 0.5475$ [W/m℃]

TABLE 2 PHYSICAL PROPERTIES OF COPPER

	ρ - (*kg/m³*)	c_p - (*J/kg.K*)	k - (*W/m.K*)
Copper	8954	384	398

DOI: 10.5963/IJEE0503002

Figs. 6 and 7 show comparisons of the numerical predictions of the interface position with experimental results for two working fluid temperatures [15]. As can be seen, the agreement is good. The solidified mass on the external side of the bent tube is more than that on the internal side. The internal heat transfer coefficient on the external side is more than that on the internal side, due to more recirculation and secondary flow effects on the external side of the bend, in agreement with [2-4]. This enhances PCM solidification on the external side.

Fig. 8 shows a photograph of solidification of the PCM around the curved tube. The solid liquid interface in the photograph is discretized, and the true physical position is calculated and plotted from the reference scale, as in Figs. 6 and 7. As was mentioned before, only the interface coincident with the symmetry line of the bend is presented in these figures. As can be observed, the interface position on the external side is more than that on the internal side.

The predicted interface velocity was compared with experimental measurements, and as can be seen in Fig. 9, the agreement is good, except for the initial instances where the numerical predictions are higher than the experimental values, due to the ideal conditions assumed in the numerical calculations. One can also observe that the interface velocity of the external side is more than that on the internal side, for the same reasons mentioned while discussing Figs. 6 and 7; this also agrees with predictions available in the literature.

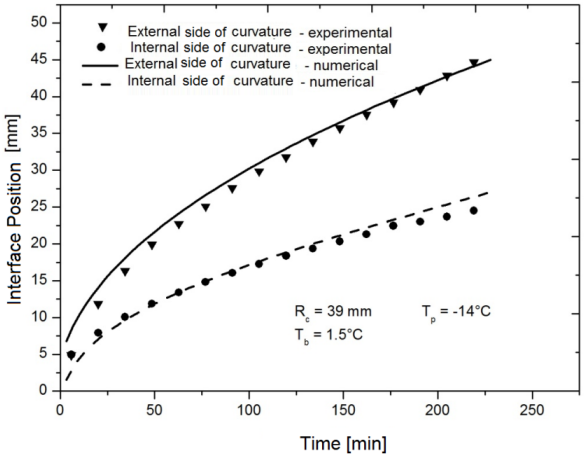

Fig. 6 Comparison between the predicted and experimental interface positions [15]

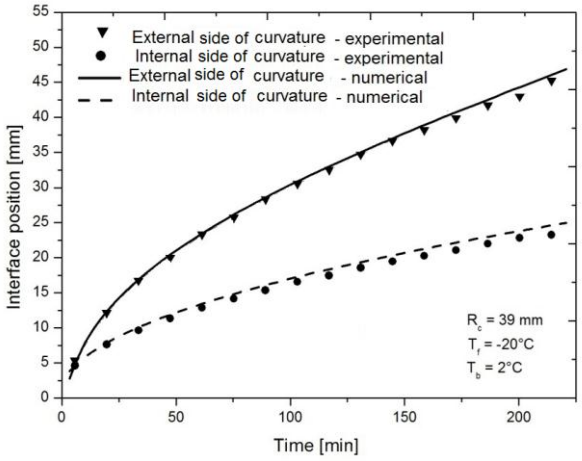

Fig. 7 Comparison between the predicted and experimental interface positions [15]

DOI: 10.5963/IJEE0503002

Fig. 8 Photograph of the interface around the bent tube

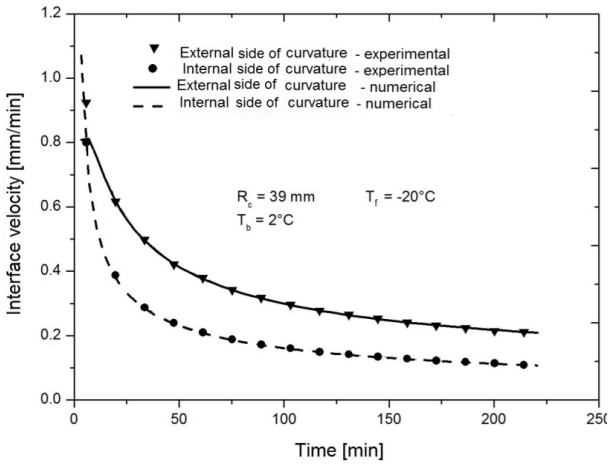

Fig. 9a Comparison between the predicted and experimental interface velocities [15]

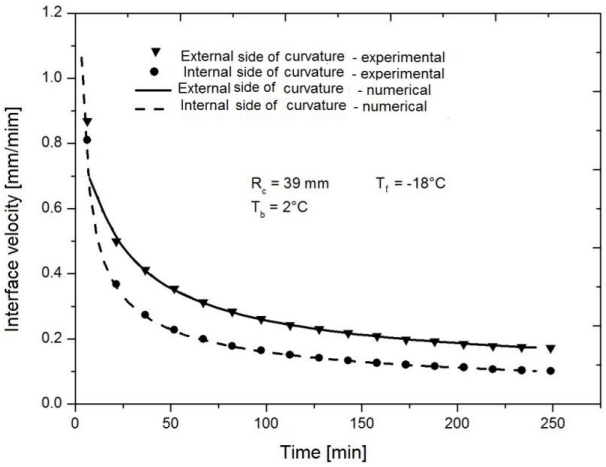

Fig. 9b Comparison between the predicted and experimental interface velocities [15]

Fig. 10 shows the variation of the dimensionless wall temperature on the internal and external sides of the bent tube, as defined by equation (13e). The variation of the dimensionless temperature along the external and internal sides of the bend is different. This difference is due to the internal circulatory flow generated by centrifugal forces acting on the circulating fluid, causing more agitation inside the bend on the external side than on the internal side. This provokes different heat transfer coefficients on the internal surface of the bend, producing lower temperatures on the external side than on the internal side, confirming the findings of [2, 4, 5]; this is also in agreement with the experimental results in Figs. 6 and 7.

Fig. 11 shows the variation of the interface position with the wall temperature. The decrease of the wall temperature increases the temperature difference between the PCM and the tube wall. This enhances the solidification rate and hence

DOI: 10.5963/IJEE0503002

increases the interface position. In Fig. 11, three initial PCM bulk temperatures were tested. The small initial PCM temperature reduces the sensible heat load (in this case), and consequently solidification is faster, and the interface position is larger.

Fig. 12 shows the effect of the wall temperature on the time for complete solidification. As expected, reducing the wall temperature reduces the time for complete solidification, due to the increase of the temperature difference between the tube wall and the surrounding PCM. Again, increasing the PCM bulk temperature strengthens the convective currents, retards the solidification process, and increases the complete solidification time, as in [21].

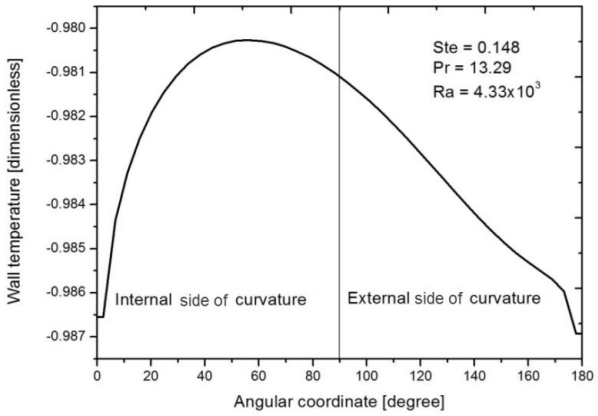

Fig. 10 Distribution of the wall dimensionless temperature along the angular coordinate

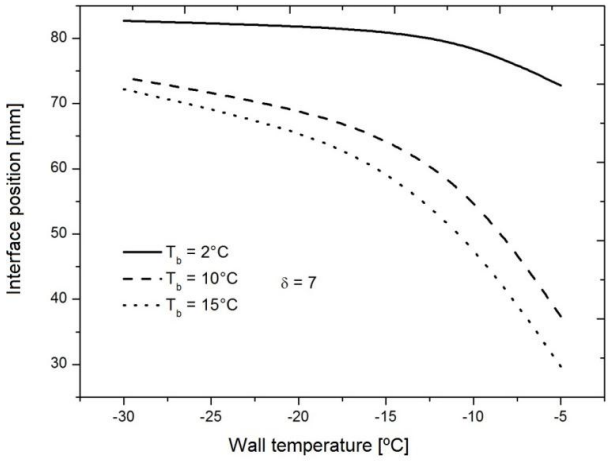

Fig. 11 Effect of wall temperature on the interface position

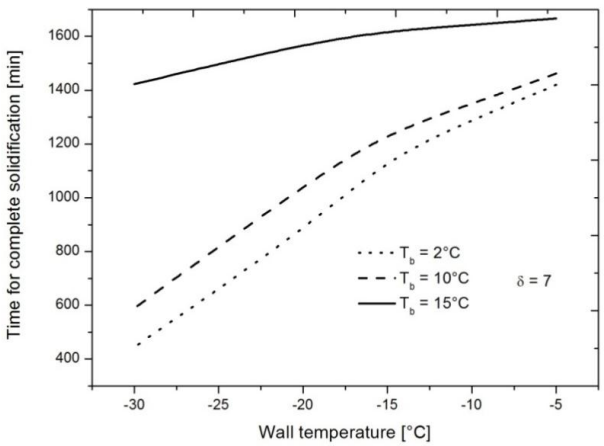

Fig. 12 Effect of wall temperature on time for complete solidification

Fig. 13 shows the effects of the initial bulk temperature of the liquid PCM on the interface position for different wall temperatures. One can observe that when the initial bulk temperature of the PCM is high, the solidification process is retarded

DOI: 10.5963/IJEE0503002

due to the large sensible heat load, which reduces the interface position. On the other hand, reducing the temperature of the circulating fluid increases the temperature difference between the cooling fluid and the PCM, enhancing the solidification rate and increasing the solidified mass.

Fig. 14 shows the effect of the initial wall temperature on the interface position for different values of the curvature ratio, $\delta=R_c / r_p$. As can be seen, increasing the value of δ reduces the amount of the solidified mass due to the reduction of the bend effects in the form of recirculation and agitation; consequently, this reduces the heat transfer coefficients. In the limit where $\delta \rightarrow\infty$, the bent tube behaves as a straight tube and the solidified mass becomes equal to that of the straight tube.

Fig. 15 shows the influence of the initial temperature of the liquid PCM on the time for complete solidification for different values of the curvature ratio. As before, when the PCM temperature is large, the temperature gradient is also large. This decreases the heat transfer rate and consequently increases the time for complete solidification. One can also observe that increasing the curvature ratio increases the time for complete solidification because of the reduction of bend effects, circulatory flow, and agitation. This reduces the heat transfer coefficients and the interface velocity.

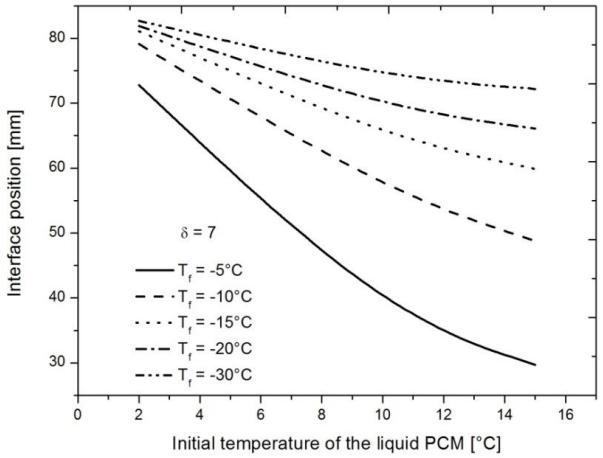

Fig. 13 Effect of the initial temperature of the liquid PCM on the interface position

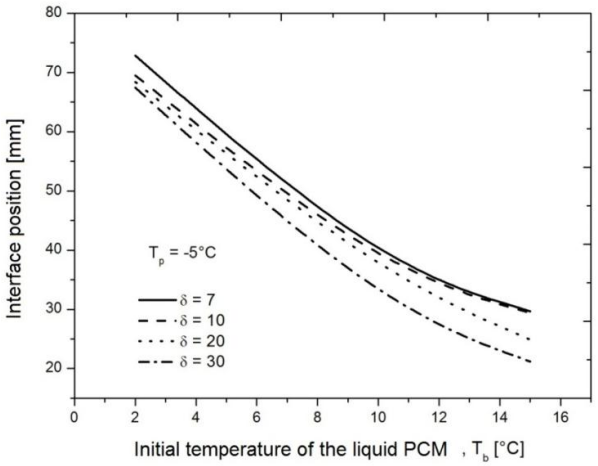

Fig. 14 Effect of the initial liquid PCM temperature on the interface position

DOI: 10.5963/IJEE0503002

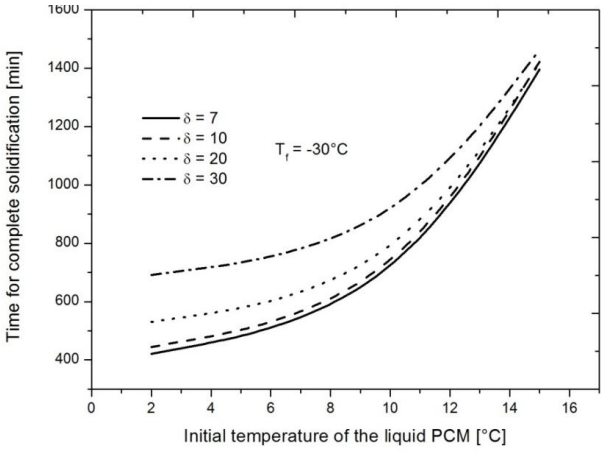

Fig. 15 Influence of the initial temperature of the liquid PCM on the time for complete solidification for different values of the curvature ratio

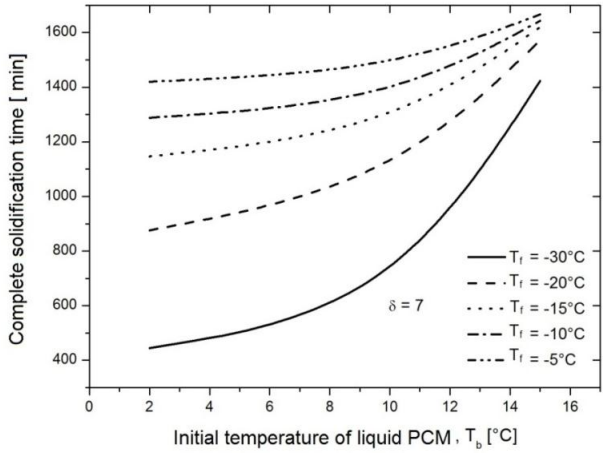

Fig. 16 Influence of the initial temperature of the liquid PCM on the time for complete solidification for different working fluid temperatures

Fig. 16 shows the effect of the initial PCM bulk temperature on the time for complete solidification for different wall temperatures. Reducing the PCM initial bulk temperature reduces the time for complete solidification since the amount of sensible heat to be removed before solidification is small. Reducing the wall temperatures enhances the solidification rate due to the increased temperature gradient between the working fluid and the PCM.

Fig. 17 shows the effect of the curvature ratio on the interface position. When the curvature ratio is small, the internal flow agitation and recirculation are more intense, causing a higher heat transfer coefficient and hence more solidification. Again, the decrease of the wall temperature increases the temperature gradient and enhances the interface position.

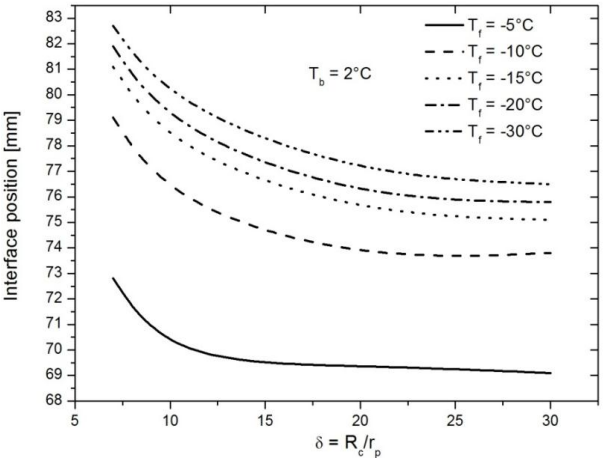

Fig. 17 Effect of the curvature ratio on the interface position

The increase of the curvature ratio increases the time for complete solidification due to the reduced flow agitation and recirculation. These effects reduce the solidification rate and thus increase the time for complete solidification.

DOI: 10.5963/IJEE0503002

Fig. 18 shows the effect of the curvature ratio, $\delta = R_c / r_p$, on the interface velocity for wall fluid temperatures. When the curvature ratio is small, the bend effects provoke agitation and recirculation flows. Consequently, the internal heat transfer coefficient and the interface velocity increase. An opposite effect can be observed for high curvature ratios. Also, as the wall temperature is reduced, the temperature gradient between the PCM and the fluid increases, enhancing the interface velocity and reducing the time for complete solidification, as shown in Fig. 19. Fig. 19 also shows that the increase of δ reduces the internal heat transfer coefficient. This leads to a reduction of the interface velocity, consequently increasing the time for complete solidification.

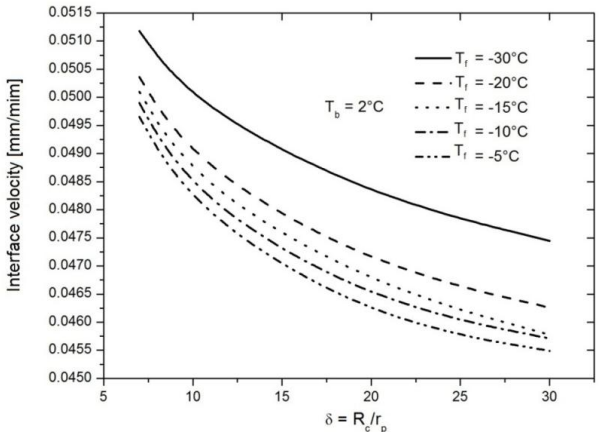

Fig. 18 Effect of the curvature ratio on the interface velocity

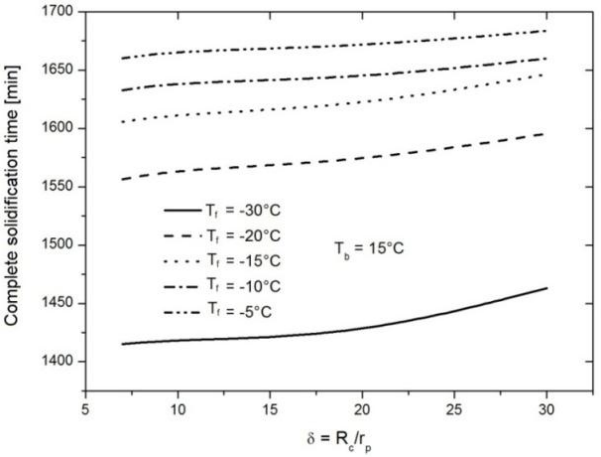

Fig. 19 Effect of the curvature ratio on the time for complete solidification

V. CONCLUSIONS

The results of the present study and comparisons with experimental results show that the model and the method of treatment by the interface immobilization technique predict results that compare well with experiments.

Because of the circulatory flow in the bend region and the associated local agitation, the heat transfer coefficient on the external side is higher than that on the internal side of the bend, causing more solidification on the external side than on the internal side of the curved tube. This increase in the heat transfer coefficient can produce variation in the solidified mass from 67% to about 90%.

A decrease in the wall temperature increases the interface position and the interface velocity and reduces the time for complete solidification. The presented results showed that reducing the wall temperature from -5^{o}C to -25^{o}C increased the interface position by nearly 95% and reduced the time for complete solidification by nearly 80%. This result is for an initial PCM bulk temperature of 10^{o}C and a curvature ratio of 7.

The increase of the initial PCM bulk temperature reduces the interface position and consequently reduces the solidified mass and the interface velocity. This increases the time for complete solidification. Varying the initial PCM bulk temperature from 2^{o}C to 12^{o}C can reduce the interface position by nearly 100% for a curvature ratio of 7 and an initial PCM bulk temperature of -5 ^{o}C. Varying the initial PCM bulk temperature from 2^{o}C to 12^{o}C increases the time for complete solidification by nearly 120%, with a curvature ratio of 7 and an initial PCM bulk temperature of -30^{o}C.

The decrease of the curvature ratio increases the interface position, increases the interface velocity, and reduces the time for complete solidification. The increase of the curvature ratio from 7 to 30 reduces the interface position by about 12%.

DOI: 10.5963/IJEE0503002

These results can be helpful in the design of bent tubes and helical coils used in energy storage systems.

ACKNOWLEDGEMENTS

The authors wish to thank FAPEMA for the Doctorate scholarship to the second author and CNPQ for the PQ Research Grant to the first author.

REFERENCES

[1] W. R. Dean, "Note on the motion of a fluid in a curved pipe," 4th ed., *Philosophical Magazine*, vol. 4, pp. 208-223, 1927.

[2] W. B. Hauwes, "Some sidelights on the heat transfer problem," 10th ed., *Trans. Inst. Chem. Engrs*, vol. 10, pp. 161-167, 1932.

[3] V. Kubair and N. R. Kuloor, "Heat transfer to newtonian fluids in coiled pipes in laminar flow," *International Journal of Heat and Mass Transfer*, vol. 9, pp. 63-75, 1966.

[4] M. N. Ozisik and H. C. Topakoglu, "Heat transfer for laminar flow in a curved pipe," *Journal of Heat Transfer*, vol. 90, pp. 313-318, 1968.

[5] C. E. Kalb and J. D. Seader, "Heat and mass transfer phenomena for viscous flow in curved circular tubes," *International Journal of Heat and Mass Transfer*, vol. 15, pp. 801-817, 1972.

[6] C. E. Kalb and J. D. Seader, "Fully developed viscous-flow heat transfer in curved circular tubes with uniform wall temperature," *AIChE Journal*, vol. 20, 1974.

[7] S. V. Patankar, V. S. E. Pratap, and D. B. Spalding, "Prediction of laminar flow and heat tranfer in helical coiled pipes," *Journal of Fluid Mechanics*, vol. 62, pp. 539-551, 1974.

[8] L. A. Janssen and C. J. Hoogendoorn, "Laminar convective heat transfer in helical coiled tubes," *International Journal of Heat and Mass Transfer*, vol. 21, pp. 1197-1206, 1978.

[9] R. Yang and S. F. Chang, "A numerical study of fully developed laminar flow and heat transfer in a curved pipe with arbitrary curvature ratio," *International Journal of Heat and Fluid Flow*, vol. 14, pp. 138-145, 1993.

[10] G. Yang and M. A. Ebadian, "Convective heat transfer in a curved annular-sector duct," *Journal of Thermo physics and Heat Transfer*, vol. 7, pp. 441-446, 1993.

[11] J. Braun and H. Beer, "Ice formation for turbulent flow in curved rectangular channel," *International Journal of Heat and Mass Transfer*, vol. 38, pp. 1505-1514, 1995.

[12] M. R. H. Nobari and E. A. Amani, "Numerical investigation of developing flow and heat transfer in a curved pipe," *International Journal of Numerical Methods for Heat & Fluid Flow*, vol. 19, pp. 847-873, 2009.

[13] K. A. R. Ismail, L. M. F. Sousa, and F. A. M. Lino, "Solidification of pcm around a curved tube," *International Journal of Heat and Mass Transfer*, vol. 55, pp. 1823-1835, 2011.

[14] J. C. Kurnia, A. P. Sasmito, S. V. Jangam, and A. S. Mujumdar, "Improved design for heat transfer performance of a novel phase change material thermal energy storage," *Applied Thermal Engineering*, vol. 50, pp. 896-907, 2013.

[15] L. M. F. Sousa, "Estudo numérico-experimental de mudança de fase em torno de tubo curvo," M. Eng. thesis, Faculty of Mechanical Engineering, State University of Campinas, 2009(in Portuguese).

[16] L. M. F. Sousa, "Estudo numérico da solidificação do PCM ao redor de tubos curvos com o efeito da convecção natural," D. Eng, thesis, Faculty of Mechanical Engineering, State University of Campinas, 2013.

[17] S. V. Patankar, Numerical Heat Transfer and Fluid Flow, Hemisphere Publishing Co., 1980.

[18] S. V. Patankar and D. B. Spalding, "A calculation procedure for heat, mass and momentum transfer in three-dimensional parabolic flows," *International Journal of Heat and Mass Transfer*, vol. 15, pp. 1787-1806, 1972.

[19] R. Viskanta, Natural Convection in Melting and Solidification, Natural Convection – Fundamentals and Applications, Hemisphere Publishing Co., 1985.

[20] E. M. Sparrow, J. W. Ramsey, and R. G. Kemink, "Freezing controlled by natural convection," *ASME Journal of Heat Transfer*, vol. 101, pp. 578-584, 1979.

[21] K. A. R. Ismail and M. E. S. Graça, "Numerical solution of the phase change problem around a horizontal cylinder in the presence of nature convection in the melt region," *International Journal of Heat and Mass Transfer*, vol. 46, pp. 1791-1799, 2003.

[22] A. Bejan, *Heat Transfer*, John Wiley & Sons, New York, 1993.

NOMENCLATURE

Latin letters

c_p: Specific heat at constant pressure [J / kg^oC]

d: Tube diameter [*m*]

g: Gravity acceleration [m/s^2]

k: Thermal conductivity [$W / m°C$]

L: Solidification latent heat [J / kg]

DOI: 10.5963/IJEE0503002

P: grid point pressure [Pa]
r_p: Tube radius [m]
r_i: Interface position [m]
rsp: Temperature coefficient
R: Dimensionless radial coordinate
R_c: Curvature radius [m]
R_1: Dimensionless radius in the solid region
R_2: Dimensionless radius in the liquid region
T: time [s]
$T_{1,2}$: Temperature of the solid and liquid phases [℃]
T_{mean}: Water bulk temperature [℃]
U: Dimensionless velocity component in the radial direction, r
V: Dimensionless velocity component in the direction, θ
V_r: Velocity component in the radial direction r [m/s]
V_θ: Velocity component in the direction θ [m/s]
$V\phi$: Velocity component in the direction ϕ [m/s]
H: Dimensionless temperature, $H = \dfrac{T - T_m}{T_m - T_p}$

Greek letters

α: Thermal diffusivity [$m^2 s^{-1}$]
β: Coefficient of thermal expansion [K^{-1}]
δ: Curvature ratio $\equiv [R_c/r_p]$
ϕ: Coordinate along circumference
Δ: Auxiliary variable, dimensionless interface thickness
η: Radial transformed coordinate
μ: Dynamic viscosity [$kgm^{-1}s^{-1}$]
ν: Kinematic viscosity [m^2s^{-1}]
θ: Angular coordinate
ρ: Specific mass [kgm^{-3}]
τ: Dimensionless time
Λ, Ω, Ψ, Θ: Auxiliary variables
$\forall$: Dimensionless volume

Subscript

i: interface
in: initial
$liquid$: liquid phase
m: phase change
$mean$: mean
nb: neighbor
p: tube wall
ref: reference
rad: relative to the r direction
$solid$: solid phase
θ: angular direction
1: solid phase
2: liquid phase

DOI: 10.5963/IJEE0503002

Dimensionless numbers

Fo: Fourier number = $\alpha t / r_p^2$

Pr: Prandtl number = ν / α

Ra: Rayleigh number for specified cylinder surface temperature = $g\beta\left(T_p - T_m\right)r_p^3 / \nu\alpha$

Ra_q: Rayleigh number for specified heat flux on the cylinder surface = $g\beta q r_p^4 / \nu\alpha k$

Ra_{agua}: Rayleigh number for specified heat flux on the cylinder surface = $grsp\left|T_m - T_p\right|^{1,894816} r_p^3 \left(\nu\alpha\left(1 - rsp\left|T_{mean} - T_{ref}\right|^{1,894816}\right)\right)^{-1}$

Ste: Stefan number for specified temperature = $c_p\left(T_m - T_p\right) / L$

Ste_q: Stefan number for specified heat flux = $c_p q r_p / Lk$

DOI: 10.5963/IJEE0503002